Cold Regions Science and Technology 110 (2015) 160–169

Contents lists available at ScienceDirect

Cold Regions Science and Technology

journal homepage: www.elsevier.com/locate/coldregions

Measuring and localizing acoustic emission events in snow prior to fracture

Ingrid Reiweger [a,*], Klemens Mayer [a,b], Kevin Steiner [a,c], Jürg Dual [c], Jürg Schweizer [a]

[a] WSL Institute for Snow and Avalanche Research SLF, Davos, Switzerland
[b] University of Technology, Graz, Austria
[c] Institute of Mechanical Systems, ETH Zürich, Switzerland

ARTICLE INFO

Article history:
Received 14 April 2014
Received in revised form 28 November 2014
Accepted 2 December 2014
Available online 10 December 2014

Keywords:
Snow
Acoustic emission
Weak layer
Fracture

ABSTRACT

Acoustic emissions (AE) are transient elastic waves produced by a sudden redistribution of stress in a material caused by changes in the internal structure. In other natural, heterogeneous materials monitoring AE has proven to be a valuable tool for stability estimation and failure prediction. After studying the characteristics of ultrasonic wave propagation in snow, we measured the acoustic emission signals during snow loading experiments in a cold laboratory. Using snow columns we found that most energy of an artificial acoustic signal was transmitted at 31 kHz. Best coupling to snow was achieved by attaching the AE sensors with silicone adhesive to thin aluminium plates which were then frozen to the snow. Localizing AE events during fracture of layered snow samples showed that the AE originated within the weakest layer, i.e. the relevant layer for snow failure. For finding an indication of imminent failure, we analysed the exponent β of the cumulative size-frequency distribution ('survival curve') of event energy. At the occurrence of instabilities, the β-curve deviated from steady behaviour and exhibited distinct 'drops', indicating that the power law behaviour of the distribution was not fulfilled anymore. Studying the temporal evolution of the exponent β might therefore provide useful information about snowpack stability also in the field—provided that the AE signals are not too strongly attenuated and can be detected in time before catastrophic failure occurs.

1. Introduction

The release of a dry-snow slab avalanche is preceded by crack formation within the snowpack (e.g. McClung and Schaerer, 2006; Schweizer et al., 2003). A weak layer, often consisting of buried surface hoar, faceted or depth hoar crystals (Schweizer and Jamieson, 2001), beneath a cohesive slab is a prerequisite for dry-snow slab avalanche release. If a macroscopic crack reaches a size of 10 cm or more it may quickly propagate in the weak layer across an entire snow slope. This process is called 'crack propagation', and, if the slope is steep enough, leads to the release of a slab avalanche. The formation of the first macroscopic 'initial' crack is called 'failure initiation' and assumed to be due to the accumulation of damage, i.e. microscopic cracks within the weak layer (Schweizer et al., 2003). Cracking on a microscopic scale is expected to always happen during snow deformation, but only if not compensated by re-bonding or sintering (e.g. Reiweger et al., 2009b; Schweizer, 1999), it is expected to lead to a macroscopic instability where larger cracks form (Schweizer et al., 2003).

Since cracking within a material is accompanied by the release of elastic energy generating elastic waves (acoustic signals), recording acoustic emissions (AE) can be used for detecting cracks and crack growth (e.g. Lockner, 1993). In other quasi-brittle materials such as concrete (Ohtsu, 1996) or wood (Bucur, 2006) the AE technique is commonly used to study and predict failure processes (Johansen and Sornette, 2000). In the field of natural hazards, acoustic signals have been used to investigate earthquake occurrence (Niccolini et al., 2011) and to predict the collapse of a limestone cliff (Amitrano et al., 2005; Got et al., 2010). Girard et al. (2012) set up an acoustic sensor network in order to predict failure within rocks and permafrost. For analyzing emissions of a glacier to anticipate the break-off of a frontal lamella, Faillettaz et al. (2011) applied a method from the framework of critical phenomena. According to the theory of critical phenomena (Johansen and Sornette, 2000) an analogy between the failure of inhomogeneous or disordered materials such as snow and a phase transition exists. The material can be considered in a stable state—microscopic cracks form but do not coalesce to form a macroscopic crack that will propagate—and an unstable state—catastrophic failure highly possible.

The application of the AE technique to snow within the context of avalanche research started in the 1970s, when several field studies for detecting acoustic activity (at frequencies ranging from 3 to 100 Hz) within the natural snow cover were performed (Gubler, 1979; Sommerfeld, 1977; St. Lawrence and Bradley, 1977). The authors concluded that avalanche formation was related to an increased acoustic activity. Bradley and St. Lawrence (1975) showed the Kaiser effect in snow based on laboratory measurements.

* Corresponding author.
E-mail address: reiweger@slf.ch (I. Reiweger).

http://dx.doi.org/10.1016/j.coldregions.2014.12.002
0165-232X/

Sommerfeld (1982) and Sommerfeld and Gubler (1983), postulated that all avalanches should be preceded by acoustic activity. St. Lawrence (1980) developed an analytical model of AE response of snow. He expressed the acoustic activity as a function of strain and stress, and succeeded to reproduce the cumulative acoustic emission curve during a slow tensile experiment at a strain rate of about $10^{-6}\,s^{-1}$ with a snow sample in the laboratory. Buser (1986), Ishida (1965), and Oura (1952) performed laboratory experiments where they measured acoustic impedance, velocity, and attenuation of snow. However, within their measurement setups they could only measure the acoustic waves travelling within the pore space and not in the ice skeleton. The frequency range studied was about 100–4000 Hz.

More recently, Scapozza et al. (2004) measured acoustic emissions in the ultrasonic range in snow during compression tests in the laboratory. They found that AE signals in snow can be measured over a wide frequency range.

A study by van Herwijnen and Schweizer (2011a,b) used geophones which had a flat frequency response from 14 to over 1000 Hz; they were looking for precursors to avalanche release. They faced difficulties identifying avalanches, not to speak of precursors, due to a lot of background noise at those low frequencies.

So far, it is not clear whether AE emissions in a weak layer under loading can be detected and whether these data include precursory information. The goal of this study was therefore to initially assess some basic properties of ultrasonic wave propagation in snow, and then to measure and localize the acoustic emission in snow during load-controlled laboratory experiments. We used the theory of critical phenomena to link the cracking processes observed in snow at the micro-scale to catastrophic failure of the whole snow sample. Our long-term goal is to exploit acoustic emissions in the framework of critical phenomena to distinguish between unstable and stable snowpacks. This would allow developing an early warning system for snow avalanches.

2. Methods

In the following, we describe the methods used for studying some of the basic acoustic properties with snow columns and to perform the loading experiments as well as the corresponding analysis methods. First we will introduce the acoustic measurement system.

2.1. Acoustic measurement system

We measured acoustic emissions (AE) and acoustic reference signals with a six channel acoustic measurement system from Physical Acoustics. The system consisted of wide band piezoelectric AE transducers (20–1000 kHz), preamplifiers (with 40 dB gain), band pass filters, digitizers, a personal computer, and the recording and analysis software AEwin. The recording devices (three 18 bit 5 MSample PCI2 A/D cards) allowed for real time waveform acquisition and feature extraction. Fig. 1 shows a basic block diagram of the AE system. The threshold was set to 28 dB. Definitions of common AE parameters and expressions such as threshold, count, amplitude, and energy can be found in Grosse and Ohtsu (2008).

2.2. Snow samples

To determine the propagation characteristics of ultrasonic signals within snow, we performed wave propagation experiments where an acoustic reference signal was sent through a snow column. The reference signal was recorded before and after travelling through the column. The free standing snow columns had a diameter of 145 mm and heights ranging from 300 to 700 mm. The snow densities ranged from 270 to 310 kg m^{-3}; the snow was characterized as rounded grains of average size 0.5 mm and medium hardness (hand hardness index 3; Fierz et al., 2009). The snow columns were prepared by sieving new snow produced by a snow machine (Schleef et al., 2014) into a plastic tube and letting it sinter for three days at −5 °C.

For the localization and loading experiments we used samples consisting of three snow layers, where the middle layer was the 'weak layer'. All samples were rectangular samples with a length of 120 mm, a width of 90 mm, and a thickness of 70 mm (35 mm top layer, 5 mm weak layer, 30 mm bottom layer). The top and bottom layers of the layered samples had a density of 260 kg m^{-3}; grain type was rounded grains, the average grain size was 0.5 mm, and hand hardness index was 3. The weak layer consisted of depth hoar crystals of 1–1.5 mm in size and was soft (hand hardness index 2; Fierz et al., 2009). For validation of the AE source localization experiments, we also performed loading experiments with uniform snow samples of dimension 120 mm × 90 mm × 50 mm. The density of the uniform samples was 200 kg m^{-3}, grain type was rounded grains, average grain size was 0.5 mm, and the snow hardness was medium (hand hardness index: 3).The production of rectangular samples, either uniform or layered, in the laboratory is described in Reiweger et al. (2010) and Reiweger et al. (2009a).

2.3. Signal propagation in snow columns

All signal propagation experiments were performed in a cold laboratory at a constant temperature of −5 °C. A free-standing snow column was used in order to avoid measuring signals which had travelled through a confining container. The experimental setup is shown in Fig. 2.

As an acoustic reference signal we used a pencil lead fracture (PLF; e.g. Grosse and Ohtsu, 2008; Higo and Inaba, 1991). The PLF signal is an impulsive signal with a flat frequency distribution, ranging approximately from 1 to 600 kHz. The PLF was applied at an aluminium plate onto which the snow column was frozen and the initial PLF signal was measured by the

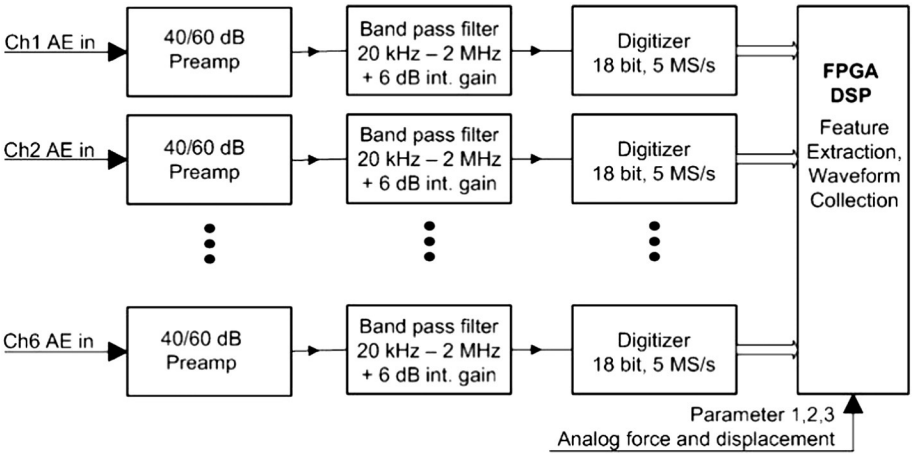

Fig. 1. Basic block diagram description of the six channel AE measurement system. The abbreviations denote Ch: channel, FPGA: field programmable gate array, and DSP: digital signal processor.

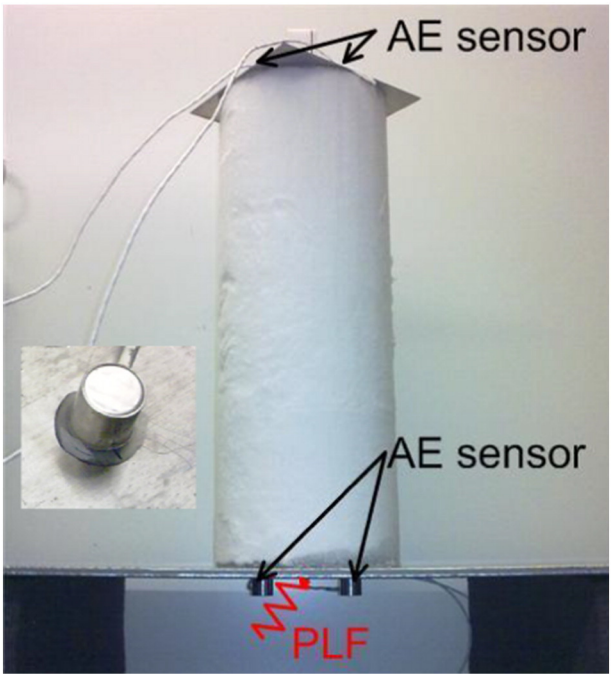

Fig. 2. Snow column for measuring the frequency response of snow column and sensors, and for evaluating the best sensor coupling. Pencil lead fracture (PLF) applied at the bottom of the column. Insert: Sensor coupled to the waveguide with silicone.

AE sensors at the bottom of the snow column. Evaluation of the signal after having travelled through the snow column (sensors at the top) should show which frequency was transmitted best.

2.4. Coupling of the sensors to the snow

As coupling of the sensors to the snow is crucial for proper signal detection, we tested direct freezing of the sensors to the snow surface as well as using different materials as couplants. For good coupling the acoustic impedance of the coupling material should be of the same order of magnitude as the acoustic impedance of snow. Snow has a very low acoustic impedance, ranging from 0.035×10^6 kg m^{-2} s^{-1} for low snow densities (125 kg m^{-3}) to 1.51×10^6 kg m^{-2} s^{-1} for high snow densities (600 kg m^{-3}) (Johnson, 1982; Lee and Rogers, 1985). We therefore used different materials with a relatively low acoustic impedance Z (Greeve and Oppenheim, 2003), i.e. plexiglass (thickness 4 mm, $Z = 3.1 \times 10^6$ kg m^{-2} s^{-1}), aluminium (thicknesses 1 mm and 5 mm, $Z = 17 \times 10^6$ kg m^{-2} s^{-1}), and foam plates (10 mm, $Z = 0.2 \times 10^6$ kg m^{-2} s^{-1}) which were frozen to the snow samples ($Z_{ice} = 2.95 \times 10^6$ kg m^{-2} s^{-1}) and glued to the sensors with silicone. The silicone's low impedance (1.51×10^6 kg m^{-2} s^{-1}) additionally reduced the reflected energy and increased the amount of transmitted AE energy from the snow to the sensor (Kapil et al., 2014). The outcome used for comparing the different coupling methods was the number of counts and the AE energy of the PLF signal having travelled through the snow column. Kapil et al. (2014) tested different geometries of aluminium waveguides for AE sensors within snow, and found that the waveguides with the largest contact area to the snow worked best. Aluminium is also a corrosion-free, lightweight, robust, and cheap material and therefore well suited for laboratory as well as field use.

2.5. Attenuation of the AE signal

Different heights of snow columns allowed calculating signal attenuation of the PLF signals within snow. Signal energy is attenuated according to

$$E = E_0\, e^{-\alpha d} \tag{1}$$

where E_0 and E are the initial energy and the energy at distance d, respectively, and α is the attenuation constant in cm^{-1}. To express the loss L_{dB} in dB, we use

$$L_{dB} = 10 \log_{10} e\, \alpha = 4.34\, \alpha. \tag{2}$$

2.6. Loading experiments

In order to study the fracture behaviour of weak snow layers, we performed loading experiments where snow samples containing a weak depth hoar layer were loaded until fracture under nature-like conditions (Reiweger et al., 2009a, 2010, 2013a). Reference measurements were also performed with uniform snow samples. The samples were loaded by the gravitational force at tilt angles of 10°, 20°, and 30° at either 'slow' loading rates of 60 or 'fast' loading rates of 150 Pa s^{-1}. A schematic of the measurement setup is shown in Fig. 3. The sensors were frozen directly to the snow samples by warming them slightly and holding them in place on the snow sample until they had firmly frozen to the sample.

2.7. Localizing acoustic emission events

To localize the acoustic emissions signals we used a localizing algorithm included in the AEwin software from Physical Acoustics. The localization algorithm is based on the different arrival times of the AE signal at different sensor locations. For three-dimensional localization the signal needs to be recorded at least at four different sensor locations. The acoustic sensors were placed in a triangular array three each in the top and the bottom plate of the sample holder (Fig. 3). The source localization of acoustic emission events is described in Grosse and Ohtsu (2008) and works similarly to earthquake localization. First, we tested the localization with artificial sources, provided by mechanical disturbance with a screwdriver and spark plug, at known locations. The second set of localization experiments included localization of AE within layered and also uniform snow samples during the loading experiments.

2.8. Analysis of AE response

We analysed the acoustic signals during the loading experiments to detect changes prior to failure that might serve as precursors. Such a change from the stable to the unstable state of a material has analogies to a phase transition. At a phase transition the material encounters a discontinuity in one of its properties, such as a jump in magnetization or the transition from solid to fluid or gas. The behaviour of material at a stable to unstable transition can be regarded in a similar manner. Phase transitions are characterized by a change of critical exponents (Johansen and Sornette, 2000). In particular, we studied the exponent

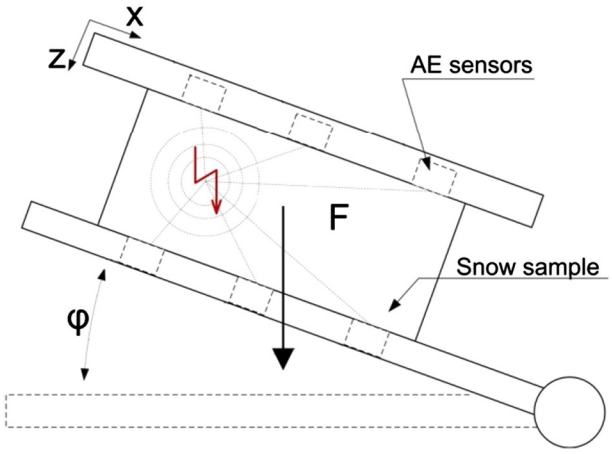

Fig. 3. Schematic test setup for loading experiments and source localization. During an experiment the force F increased, while the tilt angle ϕ remained constant. Six AE sensors measured the acoustic emissions.

β of the complementary cumulative energy distribution of acoustic events

$$p(>E) \propto E^{-\beta} \quad with \quad E \propto A^2 \tag{3}$$

where P denotes the probability that the energy E of an event is greater than a given energy. This distribution is also called 'survival curve'. The energy is proportional to the square of the amplitude A. A similar procedure was used by Faillettaz et al. (2011) to study seismic events in a hanging glacier.

We analysed the acoustic signals during the loading experiments using running time windows containing 100 events each with a distance of 50 events between subsequent time windows. Within each time window we calculated the exponent β and a level of significance p to estimate the plausibility for the power law hypothesis with an algorithm described by Clauset et al. (2009) where the fits of artificial data sets are compared to the fit of the actual data.

As an example of the complementary cumulative distribution of event energy 'survival curve' $P(>E)$, binned energy data is shown in Fig. 4. The upper plot shows the binned energy data (bins: red bars, probability: blue crosses; time window from 21.5 to 23 s, containing 100 events, sample TRA 5 in Table 1, in a linear scale. The lower plot shows the same data in a logarithmic scale with fitted power law (black). The negative slope of the fitted curve provides the exponent β of the energy distribution. The exponent β was calculated with the algorithm written and described by Clauset et al. (2009).

3. Results

3.1. Acoustic signal travelling through a snow column

The energy and number of counts which were measured after the pencil lead fracture (PLF) signal had travelled through the snow column strongly depended on the type of material used as waveguide/sensor coupling at the top of the snow column (Fig. 5). Results for the materials aluminium (thickness 1 mm), plexiglass (5 mm), and AIREX foam (10 mm) are shown in Fig. 5. The most counts and also the highest energies were measured when the sensors were attached with silicone to aluminium plates of thickness 1 mm which were frozen onto the snow.

An exemplary result of a waveform stemming from a PLF before and after travelling through the snow column is shown in Fig. 6. The original waveform (Fig. 6a) had a high amplitude and short duration, while the waveform of the signal arriving at the top of the snow column had a much smaller amplitude and longer duration (Fig. 6b). This result and all following ones were obtained using aluminium plates for sensor coupling.

Using the arrival time of the waveform at the top of the column and the column height, we calculated the acoustic velocity within the column. The wave velocities calculated from the PLF signals travelling through a snow column ranged from 300 to 550 m s^{-1}, increasing with increasing snow density as shown in Fig. 7.

The attenuation constant derived from experiments with different column heights was calculated according to Eq. 2 and was 0.05 cm^{-1}. The signal energy measured at the top of the snow column versus different column heights is shown in Fig. 8. The initial energy measured at the bottom of the snow column was 8800 μV s. The frequency spectrum of the PLF signal before and after having travelled through the snow column is shown in Fig. 9. The original signal (Fig. 9a) had almost a flat frequency distribution between 0 and 400 kHz. After having travelled through the snow column the energy decreased strongly with increasing frequency (Fig. 9b) and two clear peaks were visible at 11 and 31 kHz (Fig. 9c), indicating the least attenuation at those frequencies within our frequency spectrum that ranged from 10 to 400 kHz

3.2. Localizing the source of the acoustic events during loading experiments

Localization results from representative validation and localization experiments during loading are shown in Fig. 10. The left hand plots show a two-dimensional section of the snow sample. The green squares indicate the sensor positions, and the red dots indicate the localized AE events. In the plots on the right the energy distribution of all localized events is shown over the sample height. The first result (Fig. 10a)

Table 1
Overview of the loading experiments with layered snow samples.

Sample name	Behaviour	Tilt angle	Loading rate
LAY1	Significant drop in β at catastrophic fracture (cf)	10°	Fast
LAY2	Significant drop in β at cf; precursory fracture including drop in β	10°	Slow
LAY3	Drop in β at cf	10°	Fast
LAY4	No cf	10°	Slow
TRA1	First increase then drop in β at cf	20°	Slow
TRA2	Data acquisition defect	20°	Fast
TRA3	Sample breaks when frozen to sample holder	30°	Slow
TRA4	Significant drop in β at cf	30°	Slow
TRA5	Significant drop in β at cf (see Fig. 11)	20°	Slow
TRA6	Significant drop in β at cf; precursory fracture including drop in β (see Fig. 12)	20°	Fast
TRA7	Significant drop in β at cf	20°	Fast
TRA8	Small fracture including a drop in β; no cf	20°	Fast

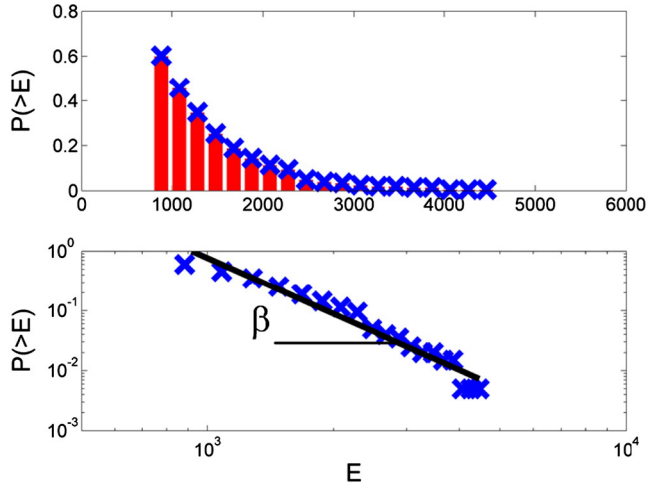

Fig. 4. Complementary cumulative distribution, 'survival curve', of event energy (arbitrary units). Top: linear scale; bottom: logarithmic scale with power law fit.

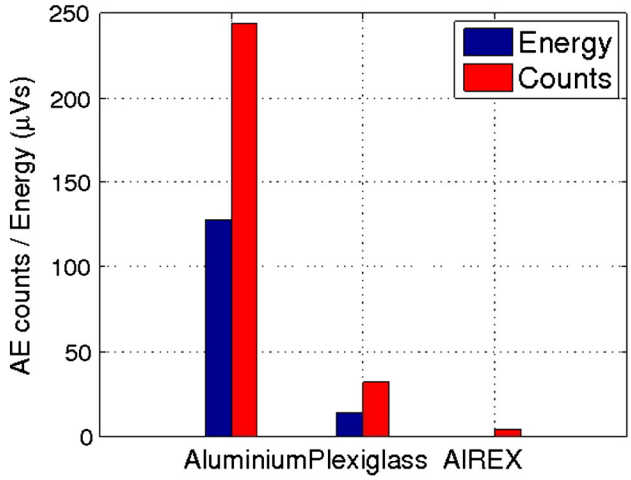

Fig. 5. AE counts and AE energy detected across waveguides made of different materials.

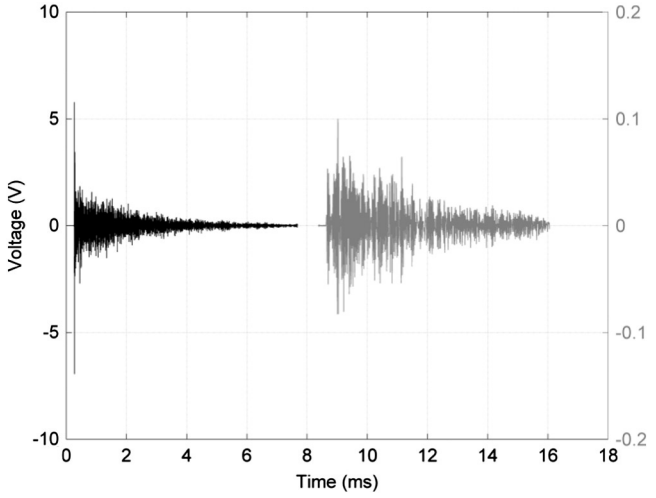

Fig. 6. Waveform before (black) and after (gray, right y-axis) travelling through the snow column, measured with aluminium waveguide, snow density 290 kg m^{-3}.

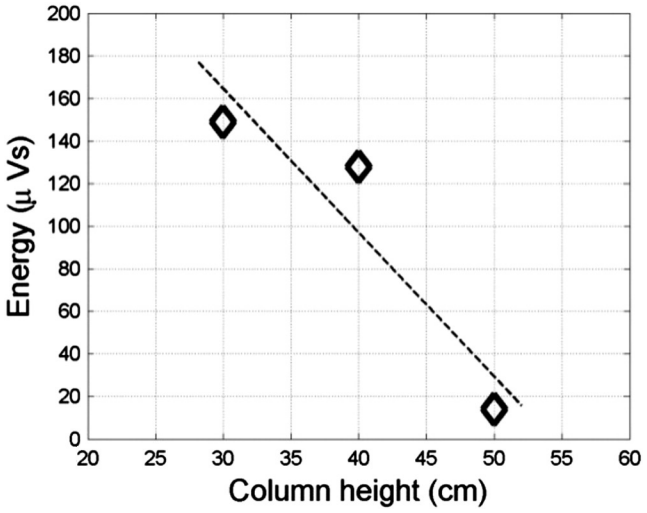

Fig. 8. Energy of the PLF signal vs. height of the snow column, measured after the signal had travelled through the column.

shows a validation experiment. The cross denotes the location of the simulated source, i.e. poking the sample with a screwdriver, surrounded by the measured AE events (red dots). The wide spreading of acoustic signals around the source is caused presumably by the indistinct nature of the applied disturbance.

During four loading experiments with layered snow samples the AE events were successfully located. The result of one of the experiments is shown in Fig. 10b. Most of the AE activity stems from the weak layer, especially regarding the AE event energy distribution. In contrast, in the case of the uniform samples (Fig. 11c), the energy distribution mostly exhibited energy peaks in the regions near the sample surfaces at the top and bottom.

Since this is the first study on localizing AE within snow, we have no other results for comparison. Looking at the different event patterns shown in Fig. 10, however, it seems that the event localization works quite well, since we see clusters of events where we expect them to be.

3.3. AE behaviour during loading experiments

We performed 12 loading experiments with layered snow samples and simultaneously measured the acoustic emissions (Table 1). For the 10 successful experiments the corresponding data are presented in Figs. 11–12, and Appendix A.

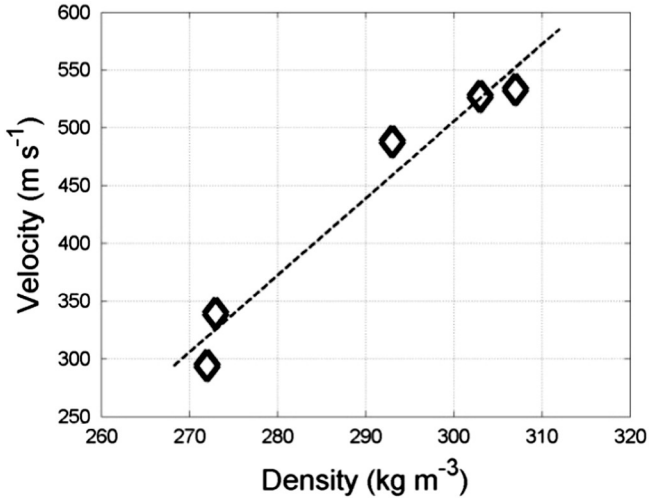

Fig. 7. Velocity of acoustic wave travelling through snow columns vs. snow density.

Fig. 11 shows a typical result of a loading experiment with a layered snow sample, i.e. counts, amplitude, and exponent β over time. The full dots mark the fits of β where the p-value was high (>0.05, see Clauset et al., 2009); for the empty circles the power law behaviour is doubtful. The counts increased during loading. Shortly before catastrophic failure the count rate accelerated, i.e. the curvature of the cumulative count rate (green line, Fig. 11a) increased. The amplitudes became significantly higher only during the fracturing, i.e. the collapse of the sample and the noise of the upper sample holder falling down (Fig. 11b). At the catastrophic failure we observed a significant decrease of β, namely $\beta < 2.5$, whereas before and after fracture β remained roughly at a constant value of 3.5 (Fig. 11c).

An example of a loading experiment including a precursor to catastrophic failure is shown in Fig. 12. After 7.5 s the weak layer partly fractured; this fracture was clearly visible by eye, and it can be considered as a precursor to catastrophic failure. The fracture was denoted 'partial' since the snow sample as a whole remained intact. This precursory fracture was also characterized by a sudden increase of the cumulative count rate and a slight decrease of the exponent β. After the fracture had occurred, the exponent β seems fairly unstable and also increases

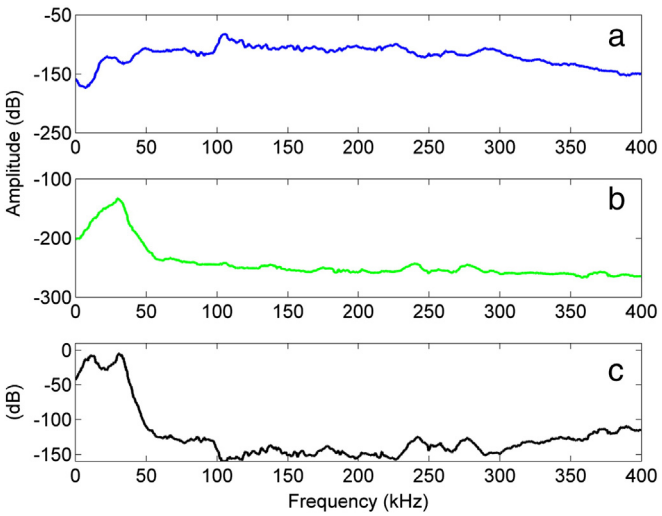

Fig. 9. Frequency spectrum of the PLF signal travelling through the snow columns. (a) Initial signal measured right next to the PLF on the aluminium plate at the bottom of the snow column. (b) Signal after having travelled through the snow column (measured at an aluminium plate at the top of the snow column). (c) Bode plot: ratio of outcoming signal (b) over initial signal (a).

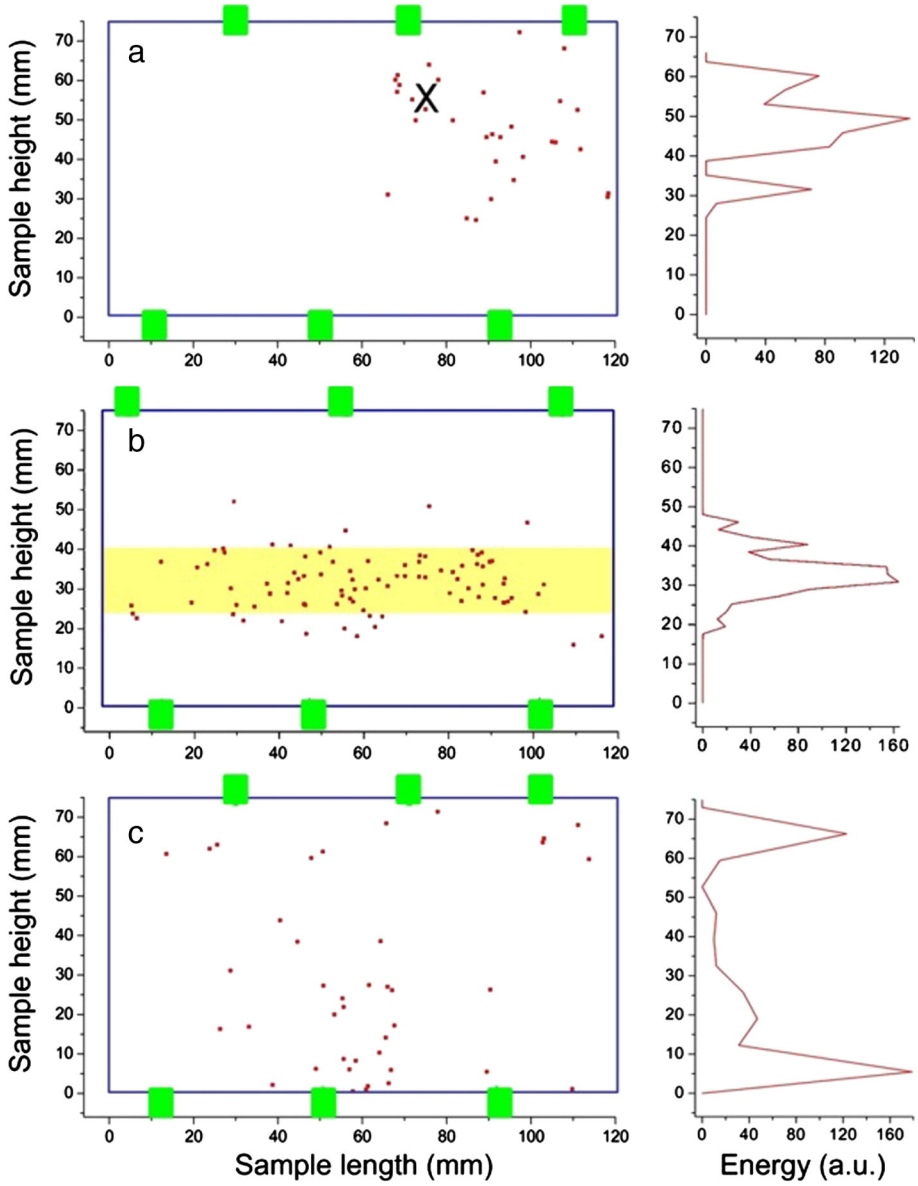

Fig. 10. Localization results from sensors at locations at the green rectangles: Plots on the left show the distribution of all localized events; the right graphs show the cumulated energy distribution for (a) a uniform sample with simulated source at the marked position (X), (b) a layered sample containing a weak layer (yellow shading; sample TRA 5, Table 1), and (c) a uniform reference sample during loading. Sample characteristics are described in Section 2. (For interpretation of the references to colour in this figure legend, the reader is referred to the web version of this article.)

again. At the catastrophic failure at $t = 22$ s, β decreased again. As in Fig. 11 the cumulative count rate and the exponent β changed during the catastrophic failure and as well at the precursory fracture, whereas no obvious change can be detected from the amplitudes only.

In all successful (i.e. 10 out of the 12) experiments with layered samples, in all that ended in catastrophic failure, we observed a drop in the exponent β before failure (Table 1). Sample TRA8 failed partly, including a drop in β, but did not exhibit obvious catastrophic failure during the experiment. In two samples (LAY2 and TRA6) we recorded a small non-catastrophic fracture and catastrophic failure shortly afterwards; all fractures were accompanied by a drop in β.

4. Discussion

Studying acoustic wave propagation within snow with our column experiments we found that thin (1 mm) aluminium plates seem a suitable waveguide material to be used with the ultrasonic sensors. This finding agrees with the observations by Kapil et al. (2014).

The waveform entering the snow sample had an amplitude that was by a factor of 50 higher than the amplitude of the out-coming waveform. While most of the energy of the initial signal was transmitted within the first 0.2 ms, within the out-coming signal the main part of the energy was spread over the first 3 ms of the signal. This is due to the dispersion—different attenuation and velocity for different frequencies—and also due to the fact that different parts of the signal may travel different paths within the highly porous material snow.

The wave propagation experiments showed that the wave velocity was of the order of the speed of sound in air c_{air} for the lower densities (about 270 kg m^{-3}) and significantly increased with increasing snow density to $c_{snow} \approx 500$ m s^{-1} for a density of 300 kg m^{-3}. The velocities measured were still small compared to the velocity of ultrasound in ice, $c_{ice} \approx 3800$ m s^{-1} (Kohnen and Gow, 1979).

The ultrasonic frequency which had the highest ratio of out-coming over initial signal (maximum of Bode plot, Fig. 9) was 30 kHz. This frequency is presumably a function of snow density and grain shape. The resonance frequency of the aluminium plates used as waveguide

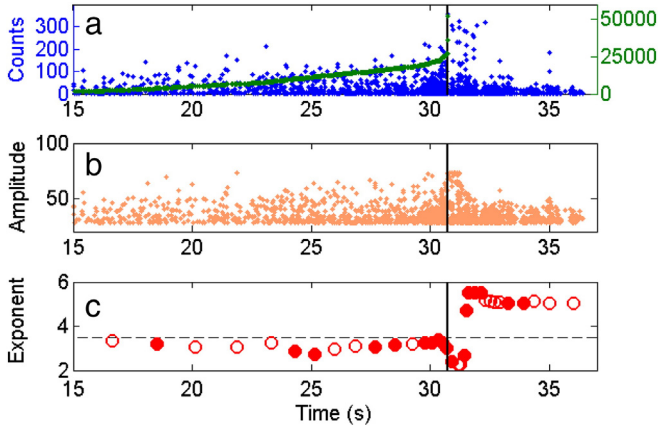

Fig. 11. (a) Counts, cumulated counts (right axes), (b) amplitude, and (c) exponent β (of the complementary cumulative event energy distribution) over time for a loading experiment with a layered snow sample (sample TRA 5, Table 1, for snow characterization see Section 2). The black vertical line marks the time of catastrophic failure. (For interpretation of the references to colour in this figure legend, the reader is referred to the web version of this article.)

was calculated to be 200 Hz, which is far away from the ultrasonic frequencies we used. We consequently assume no artefacts stemming from the geometries of the plates. However, we cannot exclude dispersive processes due to our measurement setup, e.g. coupling of sensor to the snow, completely.

Wave propagation experiments with different heights of snow columns allowed us to calculate the attenuation of the PLF signal. The attenuation constant of 0.05 cm^{-1} was converted to a loss L_{dB} of 0.22 dB cm^{-1} (Eq. 3). This value is similar to the ones reported by Iwase et al. (2001) who obtained values in the range of 0.3 to 1.5 dB cm^{-1} at frequencies from 0.1 to 5 kHz. Iwase et al. (2001) showed that attenuation increases with increasing frequency. We assume that the reason we measured a slightly smaller attenuation than Iwase et al. (2001) but at higher frequencies (10–500 kHz) is related to the fact that we performed our measurements within a snow column, where the energy has less opportunity to dissipate. Iwase et al. (2001) measured signal attenuation within a natural snowpack, which corresponds to a half-space where dissipation is expected to be large. The high attenuation of the acoustic emissions within snow suggests that for field application the sensors must be placed close to the weak layer which is expected to fail in order to measure meaningful precursors to slab avalanche release.

Measuring acoustic emissions during loading experiments clearly showed that the AE truly come from the weak layer where the failure is expected to occur. This finding is in agreement with the results by Walters and Adams (2014) as well as Reiweger and Schweizer (2010) who showed that most of the shear strain was concentrated in the weak layer. This is essentially important for the potential use of AE as precursory information to slab avalanche release. The localization results shown stem from the period before catastrophic failure (time < 30.5 s). During fracture the upper sample holder with three acoustic sensors (Fig. 3) moved and therefore localization was no longer possible. Comparing the localization results (Fig. 10) and the mere counts versus time of the same experiment (Fig. 11) it is evident that not all counts contributed to localized events. A localizable event needs to be recorded by at least four sensors (for three-dimensional localization), while a count just needs to be recorded by one sensor. So it is evident that there will always be more counts than events (acoustic waves recorded by at least four sensors), since not all acoustic emissions reach four or more sensors. Sensor coupling without a waveguide is a sensitive issue within snow, and during the loading experiments when not all sensors coupled well, localization was not possible. For small scale laboratory experiments waveguides are too large to enable source localization; for potential field use source localization using waveguides for sensor coupling should be possible since the dimensions of the wave guide are small compared to the distances of the sensors and the source. During the localization experiments with the uniform samples we measured most events relatively close to the sample holders (Fig. 10). We assume that this was due to the fact that events near the sensor are possibly rather recognized and because the stresses inside a homogeneous snow sample might be unevenly distributed, increasing near the connection between the snow and the sample holders.

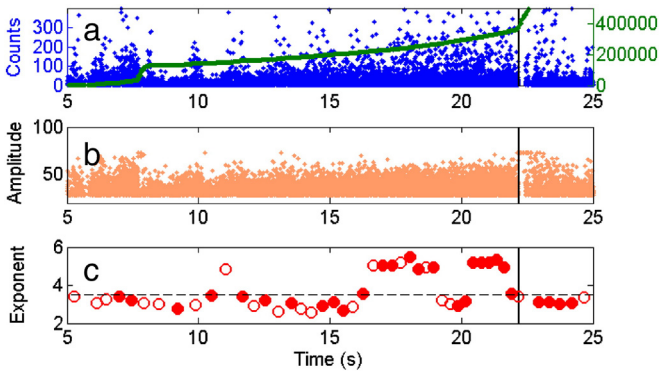

Fig. 12. (a) Counts, cumulated counts (right axis), (b) amplitude, and (c) exponent β (of the complementary cumulative event energy distribution) over time for a loading experiment with a layered snow sample (sample TRA 6, Table 1, for snow characterization see Section 2). At $t = 7.5$ s partial fracture of the sample was observed. The black vertical line marks the time of catastrophic failure.

For the acoustic emissions we measured during the loading experiments we analysed the exponent β of the complementary cumulative distribution of event energy (Eq. 3) in a running time window as described in Section 2. At catastrophic failure of our small laboratory samples (Table 1, Fig. 11, and Appendix A), and in two cases also at a precursory, non-catastrophic failure (Table 1 and Fig. 12), we observed a drop in exponent β. This drop is related large scale events, i.e. events with a larger energy take place close to catastrophic or almost-catastrophic (i.e. precursory) failure. The sudden drop of β during fracture at laboratory scale might have the potential to serve as precursor to snow failure even at large scale, e.g. in the field. For our small scale laboratory experiments the drop in β mostly occurred just fractions of a second prior to catastrophic fracture. In the two cases of precursory failure, the time span between the first drop in β and the catastrophic fracture was 15 s and 20 s, respectively. Since it takes more and larger cracks to catastrophically fracture a snow slope, we assume that at a larger length scale also the time scale might increase. In that sense our laboratory results confirm our hypothesis that AE may be a powerful tool for developing a warning system for snow avalanche release. During field measurements of seismic activity of the Weisshorn glacier (Switzerland) before break-off, Faillettaz et al. (2011) first observed an increase and then also a sudden drop of exponent β. Dalban Canassy et al. (2012) obtained similar results studying precursors to glacier break-off at the Trift glacier (Switzerland).

5. Conclusions and outlook

We performed cold laboratory experiments with snow columns to derive some basic characteristics of ultrasonic wave propagation in snow and subsequently monitored acoustic emission activity during force-controlled loading experiments with uniform and layered snow samples containing a weak layer.

The column experiments suggest that the best coupling of the AE sensors with snow can be obtained when they are attached with silicone to aluminium plates which are frozen onto the snow. Using a pencil lead fracture (PLF) as acoustic reference signal revealed that at 30 kHz most energy travelled through the columns in our experimental setup.

During the loading experiments with layered samples we succeeded for the first time to show that the acoustic emissions stem from a

fracturing weak snow layer where—as has previously been shown (Reiweger and Schweizer, 2010; Walters and Adams, 2014)—most of the deformation is concentrated. In all experiments that led to catastrophic failure, analysis of the acoustic data revealed a decrease of the exponent β of the complementary cumulative distribution of event energy during and sometimes also before catastrophic failure, at least for laboratory size samples. This drop of exponent β at and before fracture is believed to have the potential to serve as an indicator of unstable conditions—i.e. indicate a snowpack state when the avalanche release probability is high.

Both the successful localization and the change in exponent β are considered important steps towards recognition of precursors to snow failure with respect to dry-snow slab avalanche release. Based on the laboratory results a field study was designed to monitor weak layer stability in an avalanche release zone. Preliminary results were encouraging (Reiweger and Schweizer, 2013b). Based on their field experiments and the laboratory results presented here, we will continue to exploit acoustic emission measurements within snow in view of developing an early warning system for snow avalanches.

Acknowledgements

We thank Stephan Simioni for help with the experiments and Joachim Sell (Mistras Group) for advice on the acoustic measurement system and data interpretation.

Appendix A

In this Appendix the data of the nine loading experiments with layered samples (Table 1) not previously shown are presented. The sample name is given right under the figure. The different graphs show counts, amplitude, exponent β (of the complementary cumulative event energy distribution), and load over time for loading experiments with the layered snow samples (from top to bottom). The vertical line marks the time of catastrophic failure.

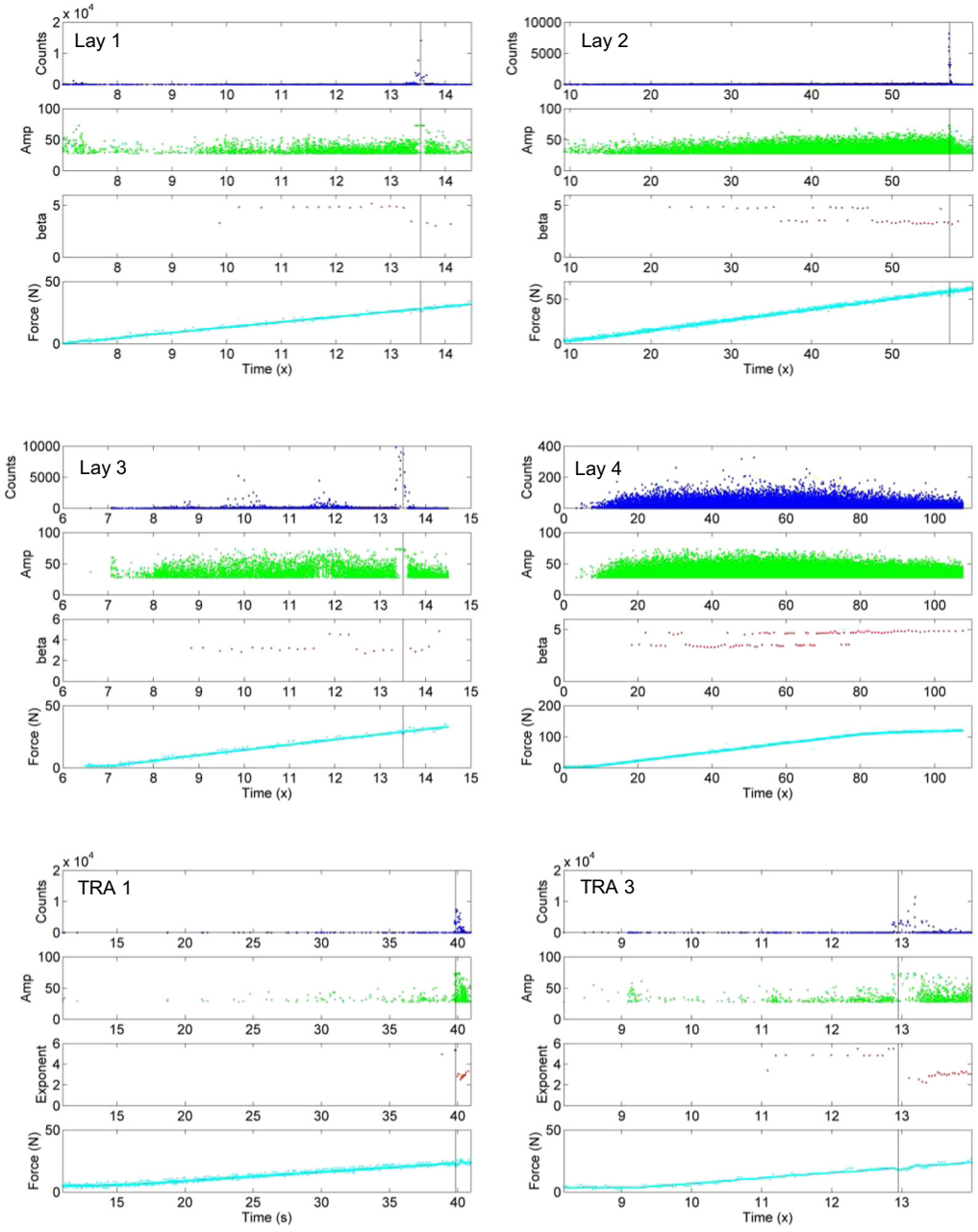

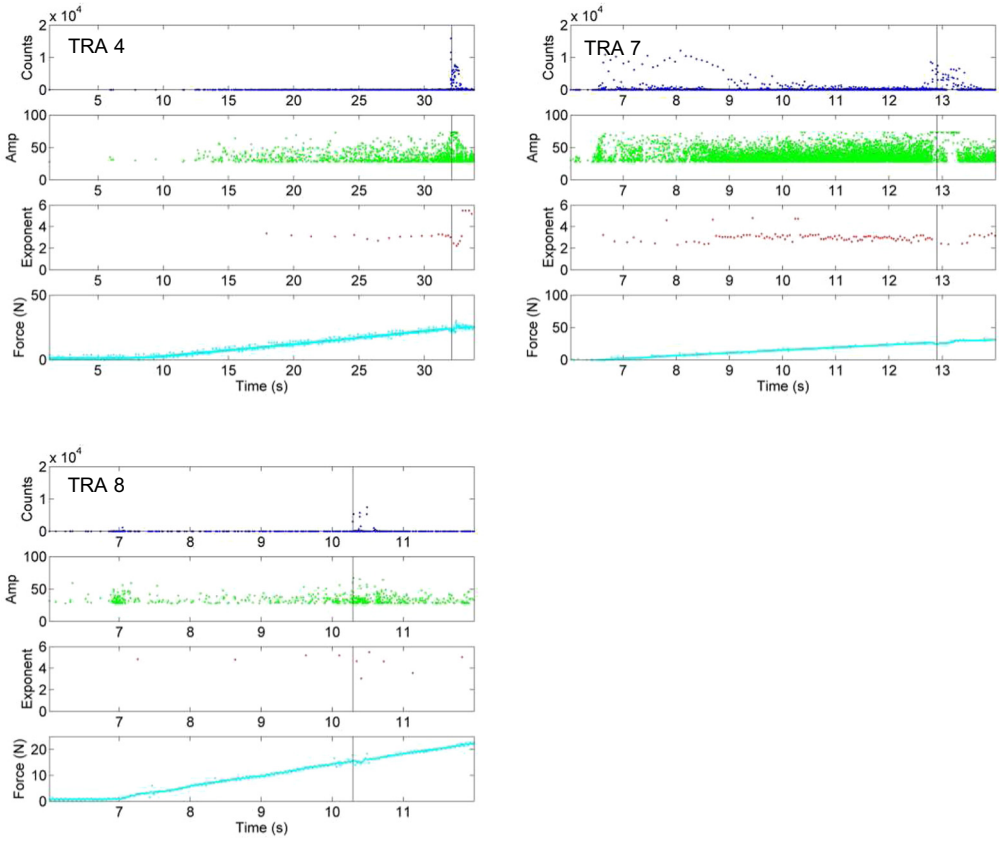

References

Amitrano, D., Grasso, J., Senfaute, G., 2005. Seismic precursory patterns before a cliff collapse and critical point phenomena. Geophys. Res. Lett. 32 (L08314).

Bradley, C., St. Lawrence, W., 1975. Kaiser effect in snow. IAHS Publ. 114, 145–154.

Bucur, V., 2006. Acoustics of Wood. 2nd edition. Springer, Berlin.

Buser, O., 1986. A rigid frame model of porous media for the acoustic impedance of snow. J. Sound Vib. 111 (1), 71–92.

Clauset, A., Shalizi, C., Newman, M., 2009. Power-law distributions in empirical data. SIAM Rev. 51 (4), 661–703.

Dalban Canassy, P., Faillettaz, J., Walter, F., Huss, M., 2012. Seismic activity and surface motion of a steep temperate glacier: a study on Triftgletscher, Switzerland. J. Glaciol. 58 (209), 513–528.

Faillettaz, J., Funk, M., Sornette, D., 2011. Icequakes coupled with surface displacements for predicting glacier break-off. J. Glaciol. 57 (203), 453–460.

Fierz, C., Armstrong, R., Durand, Y., Etchevers, P., Greene, E., McClung, D., Nishimura, K., Satyawali, P., Sokratov, S., 2009. The International Classification for Seasonal Snow on the Ground. IHP-VII Technical Documents in Hydrology. 83. UNESCO-International Hydrological Program, Paris (90 pp).

Girard, L., Beutel, J., Gruber, S., Hunziker, J., Lim, R., Weber, S., 2012. A custom acoustic emission monitoring system for harsh environments: application to freezing-induced damage in alpine rock-walls. Geoscientific Instrumentation, Methods and Data Systemspp. 267–300.

Got, J.-L., Mourot, P., Grangeon, J., 2010. Pre-failure behaviour of an unstable limestone cliff from displacement and seismic data. Nat. Hazards Earth Syst. Sci. 10, 819–829.

Greeve, D.W., Oppenheim, I.J., 2003. Coupling of MEMS ultrasonic transducers. Sensors, 2003. Proceedings of IEEE 2, pp. 814–819.

Grosse, C., Ohtsu, M., 2008. Acoustic Emission Testing. Springer, Heidelberg.

Gubler, H., 1979. Acoustic emission as an indication of stability decrease in fracture zones of avalanches. J. Glaciol. 22 (86), 186–188.

Higo, Y., Inaba, H., 1991. The general problems of AE sensors. In: Sachse, W., Roger, J., Yamaguchi, K. (Eds.), Acoustic Emission: Current Practice and Future Directions, ASTM STP 1077. American Society for Testing and Materials, Philadelphia, U.S.A., pp. 7–24.

Ishida, T., 1965. Acoustic properties of snow. Contribution from the Institute of Low Temperature Science. 20 pp. 23–63.

Iwase, T., Sakuma, K., Yoshihisa, K., 2001. Measurements on sound propagation characteristics in snow layer. Proceedings in CD-ROM of internoise 2001.

Johansen, A., Sornette, D., 2000. Critical ruptures. Eur. Phys. J. B 18, 163–181.

Johnson, J.B., 1982. On the application of Biot's theory to acoustic wave propagation in snow. Cold Reg. Sci. Technol. 6 (1), 49–60.

Kapil, J.C., Datt, P., Kumar, A., Singh, K., Kumar, V., Satyawali, P.K., 2014. Multi-sensor couplers and waveguides for efficient detection of acoustic emission behavior of snow. Cold Reg. Sci. Technol. 101, 1–13.

Kohnen, H., Gow, A.J., 1979. Ultrasonic velocity investigations of crystal anisotropy in deep ice cores from Antarctica. J. Geophys. Res. Oceans 84 (C8), 4865–4874.

Lee, S.M., Rogers, J.C., 1985. Characterization of snow by acoustic sounding: a feasibility study. J. Sound Vib. 99 (2), 247–266.

Lockner, D., 1993. The role of acoustic emission in the study of rock fracture. Int. J. Rock Mech. Min. Sci. Geomech. Abstr. 30 (7), 883–899.

McClung, D.M., Schaerer, P., 2006. The Avalanche Handbook. The Mountaineers Books, Seattle WA, U.S.A. (342 pp).

Niccolini, G., Carpinteri, A., Lacidogna, G., Manuello, A., 2011. Acoustic emission monitoring of the Syracuse Athena Temple: scale invariance in the timing of ruptures. Phys. Rev. Lett. 106, 108503.

Ohtsu, M., 1996. The history and development of acoustic emissions in concrete engineering. Mag. Concr. Res. 48 (177), 321–330.

Oura, H., 1952. Sound velocity in the snow cover. Low Temperature Science. Series A. J. Phys. Sci. 9, 171–178 (in Japanese with English summary).

Reiweger, I., Schweizer, J., 2010. Failure of a layer of buried surface hoar. Geophys. Res. Lett. 37 (L24501).

Reiweger, I., Schweizer, J., 2013a. Weak layer fracture: facets and depth hoar. Cryosphere 7 (5), 1447–1453.

Reiweger, I., Schweizer, J., 2013b. Measuring acoustic emissions in an avalanche starting zone to monitor snow stability. Proceedings International Snow Science Workshop. Grenoble, France, 7–11 October 2013.

Reiweger, I., Schweizer, J., Dual, J., Hermann, H.J., 2009a. Modelling snow failure with a fibre bundle model. J. Glaciol. 55 (194), 997–1002.

Reiweger, I., Ernst, R., Schweizer, J., Dual, J., 2009b. Force-controlled shear experiments with snow samples. In: Schweizer, J., van Herwijnen, A. (Eds.), Proceedings International Snow Science Workshop, Davos, Switzerland, 27 September–2 October 2009. Swiss Federal Institute for Forest, Snow and Landscape Research WSL, pp. 120–123.

Reiweger, I., Schweizer, J., Ernst, R., Dual, J., 2010. Load-controlled test apparatus for snow. Cold Reg. Sci. Technol. 62 (2–3), 119–125.

Scapozza, C., Bucher, F., Amann, P., Ammann, W., Bartelt, P., 2004. The temperature- and density-dependent acoustic emission response of snow in monoaxial compression tests. Ann. Glaciol. 38, 291–298.

Schleef, S., Jaggi, M., Löwe, H., Schneebeli, M., 2014. An improved machine to produce nature-identical snow in the laboratory. J. Glaciol. 60 (219), 94–102.

Schweizer, J., 1999. Review of dry snow slab avalanche release. Cold Reg. Sci. Technol. 30 (1–3), 43–57.

Schweizer, J., Jamieson, J.B., 2001. Snow cover properties for skier triggering of avalanches. Cold Reg. Sci. Technol. 33 (2–3), 207–221.
Schweizer, J., Jamieson, J.B., Schneebeli, M., 2003. Snow avalanche formation. Rev. Geophys. 41 (4), 1016.
Sommerfeld, R., 1977. Preliminary observations of acoustic emissions preceding avalanches. J. Glaciol. 19 (81), 399–409.
Sommerfeld, R., 1982. A review of snow acoustics. Rev. Geophys. Space Phys. 20, 62–66.
Sommerfeld, R., Gubler, H., 1983. Snow avalanches and acoustic emissions. Ann. Glaciol. 4, 271–276.
St. Lawrence, W., 1980. The acoustic emission response of snow. J. Glaciol. 26 (94), 209–216.
St. Lawrence, W., Bradley, C., 1977. Spontaneous fracture initiation in mountain snowpacks. J. Glaciol. 19 (81), 411–417.
van Herwijnen, A., Schweizer, J., 2011a. Monitoring avalanche activity using a seismic sensor. Cold Reg. Sci. Technol. 69 (2–3), 165–176.
van Herwijnen, A., Schweizer, J., 2011b. Seismic sensor array for monitoring an avalanche start zone: design, deployment and preliminary results. J. Glaciol. 57 (202), 267–276.
Walters, D.J., Adams, E.E., 2014. Quantifying anisotropy from experimental testing of radiation recrystallized snow layers. Cold Reg. Sci. Technol. 97, 72–80.